



Project No. Coll – Ct - 2003 - 500291

ESECMaSE

Enhanced Safety and Efficient Construction of Masonry Structures in Europe

Horizontal Research Activities Involving SMEs

Collective Research

Work Package N° 8

D 8.3 Earthquake tests and analysis of the experimental results

Due date of deliverable: 10/11/2007

Actual submission date: 04/07/2008

Start date of project: 10 June 2004

Duration: 48 months

Armelle Anthoine and Philippe Capéran
European Laboratory for Structural Assessment (ELSA)
Joint Research Centre of the European Commission
21020 Ispra (VA)

Draft N°1

Project co-funded by the European Commission within the Sixth Framework Programme (2002-2006)		
Dissemination Level		
PU	Public	
PP	Restricted to other programme participants (including the Commission Services)	X
RE	Restricted to a group specified by the consortium (including the Commission Services)	
CO	Confidential, only for members of the consortium (including the Commission Services)	

1. INTRODUCTION

The objective of WP8 is to verify the earthquake performance of a selected type of masonry building. This is to be achieved through the seismic testing of a full-scale model at the ELSA Reaction-wall Laboratory of the JRC, using the pseudo-dynamic testing technique.

This report completes the description of the testing set-up given in D8.1 (actual vertical loading conditions and instrumentation), gives the input parameters of the pseudo-dynamic tests (base accelerogram, mass matrix and damping) and presents the results of the pseudo-dynamic testing sequence for both the calcium silicate and clay specimens. Finally, the optical measurement technique operated at ELSA is presented and illustrated.

2. TESTING SET-UP

2.1. Actual vertical loading conditions

As mentioned in deliverable D8.1, the pseudo-dynamic tests should be carried out under the vertical loading conditions used in the seismic design, that is, under the dead loads and 30% of the live loads. To reproduce these conditions in the laboratory, a distribution of water tanks on each floor of the specimens has been studied which accounts for the missing dead and live loads and for the testing set-up. The masses inherent to the testing set-up correspond to:

- The additional steel reinforcement of the floor slabs in correspondence to the attachment of the actuators $\rightarrow 2 \times 114$ kg per slab,
- The post-tensioned bars and associated reinforcement $\rightarrow 223$ kg per slab
- The steel plates on which the actuators are attached $\rightarrow 2 \times 426$ kg per slab,
- The half mass of each hydraulic actuator. In reality, the actuators acting on the unsupported edge of the slabs have been counterbalanced so as to avoid an excessive bending of the slabs (Figure 1) $\rightarrow 700$ kg per slab only on the sides supported by the slender masonry walls.
- The safety frames $\rightarrow 3 \times 315$ kg on the first floor only.

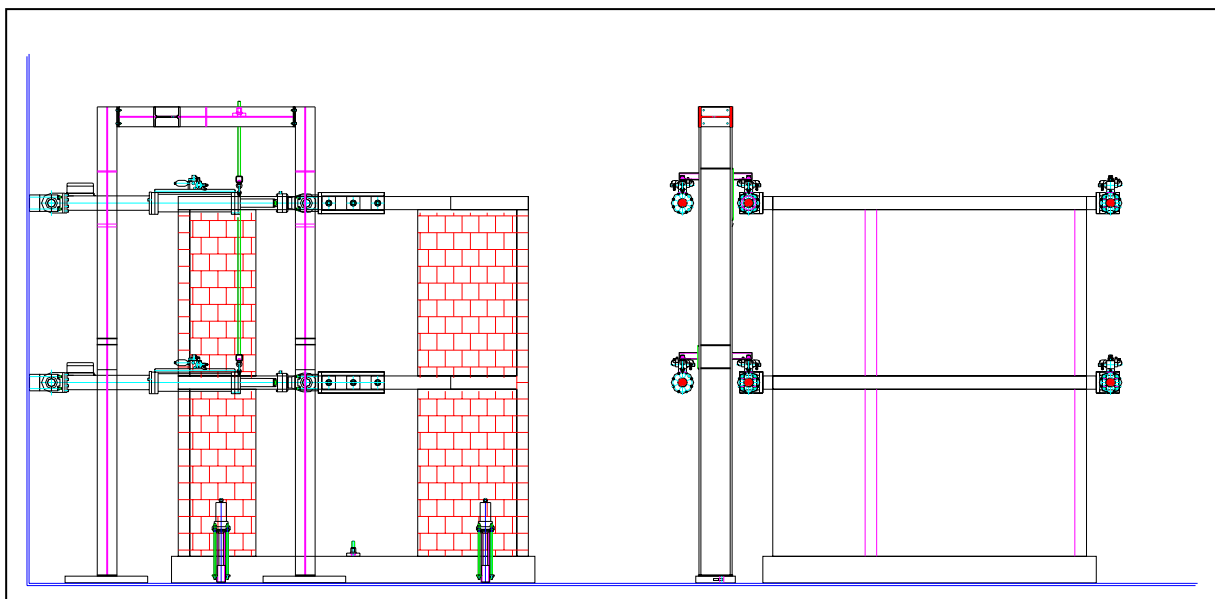


Figure 1– Balancing system for the actuators

Also, the additional mass corresponding to the higher thickness of the concrete floors should be taken into account:

- For the calcium silicate specimen, +2cm on each slab → 1128 kg per slab,
- For the clay specimen, +3.5cm and +1.5cm on the first and second floor → 1974kg and 846kg on the first and second floor respectively.

In a first step, the positions and masses of the water tanks have been determined so as to reproduce the desired vertical resultant and resulting moments acting on each floor. In a second step, the vertical stresses induced in the masonry walls have been computed on a finite element model of the specimen, both in the “theoretical” configuration (half house with distributed additional loads and symmetry conditions) and in the “practical” one (half house with concentrated additional loads and without symmetry conditions). The results were quite similar, owing to the relatively high stiffness of the floor slabs, which ensures a uniform distribution of the weight of the water tanks as well as a limited rotation at the symmetry section (see Deliverable D8.1). The final distribution of the water tanks together with the added masses inherent to the testing set-up are given in Figure 2 for the calcium silicate specimen and in Figure 3 for the clay specimen (values in kg).

2.2. Instrumentation

The final lay-out of the instrumentation is shown on Figure 4 for the calcium silicate specimen and on Figure 5 for the clay specimen. For each shear wall, the instrumentation was as much as possible similar to the one used in Pavia (Deliverable D7.1c). The main shear wall of the ground floor was also monitored by photogrammetry on the side of the staircase. Unfortunately, the second camera that should have one of the slender walls of the ground floor broke down during the first tests on the calcium silicate specimen. The long transversal walls were equipped with inclinometers and vertical displacement transducers positioned between each concrete slab and the second layer of bricks above and/or below. Besides the four transducers controlling the PsD degrees of freedom, six additional transducers have been installed to check the fixity of the base slab and the possible lateral displacements of the slabs.

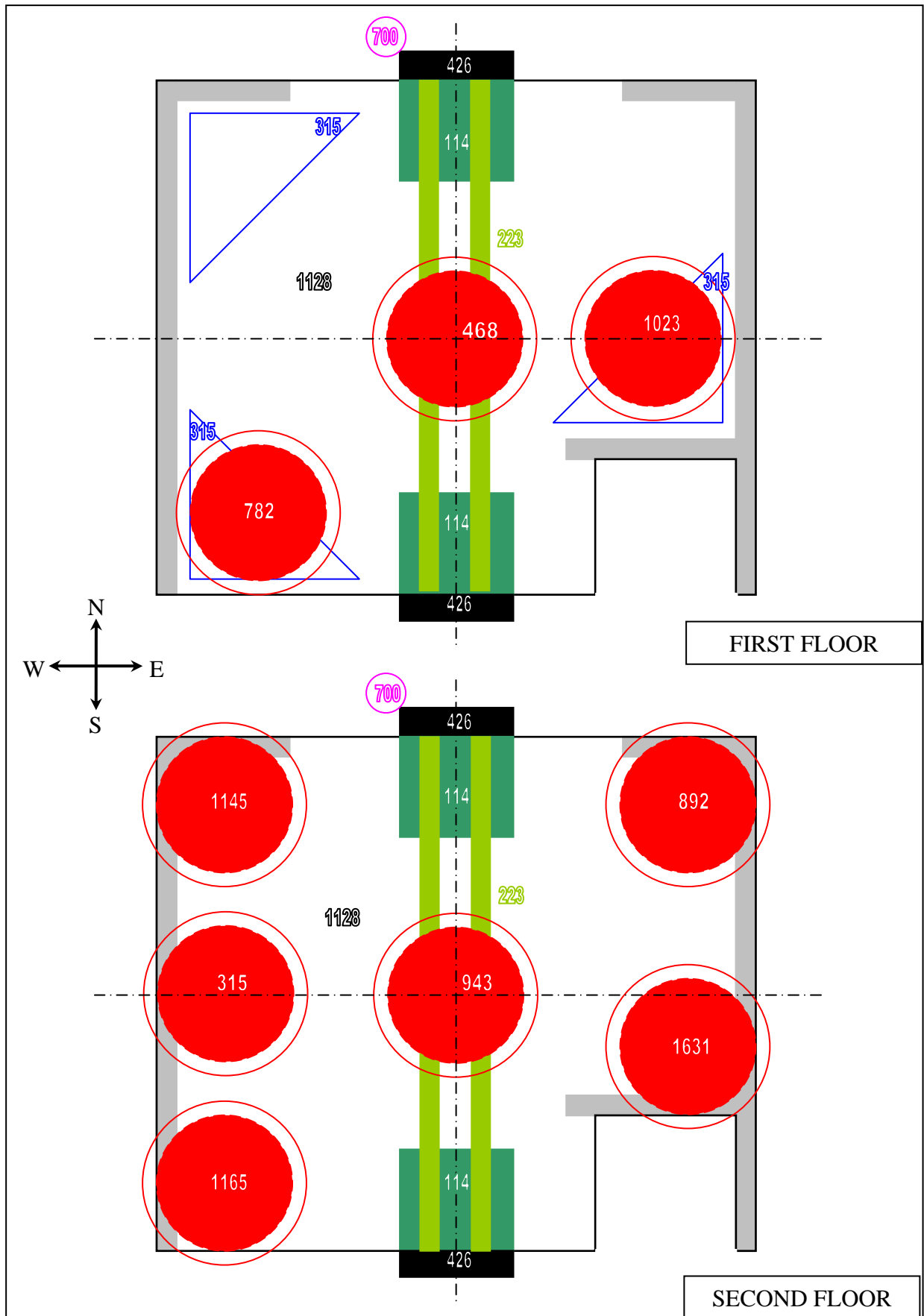


Figure 2– Distribution of the water tanks on the calcium silicate specimen

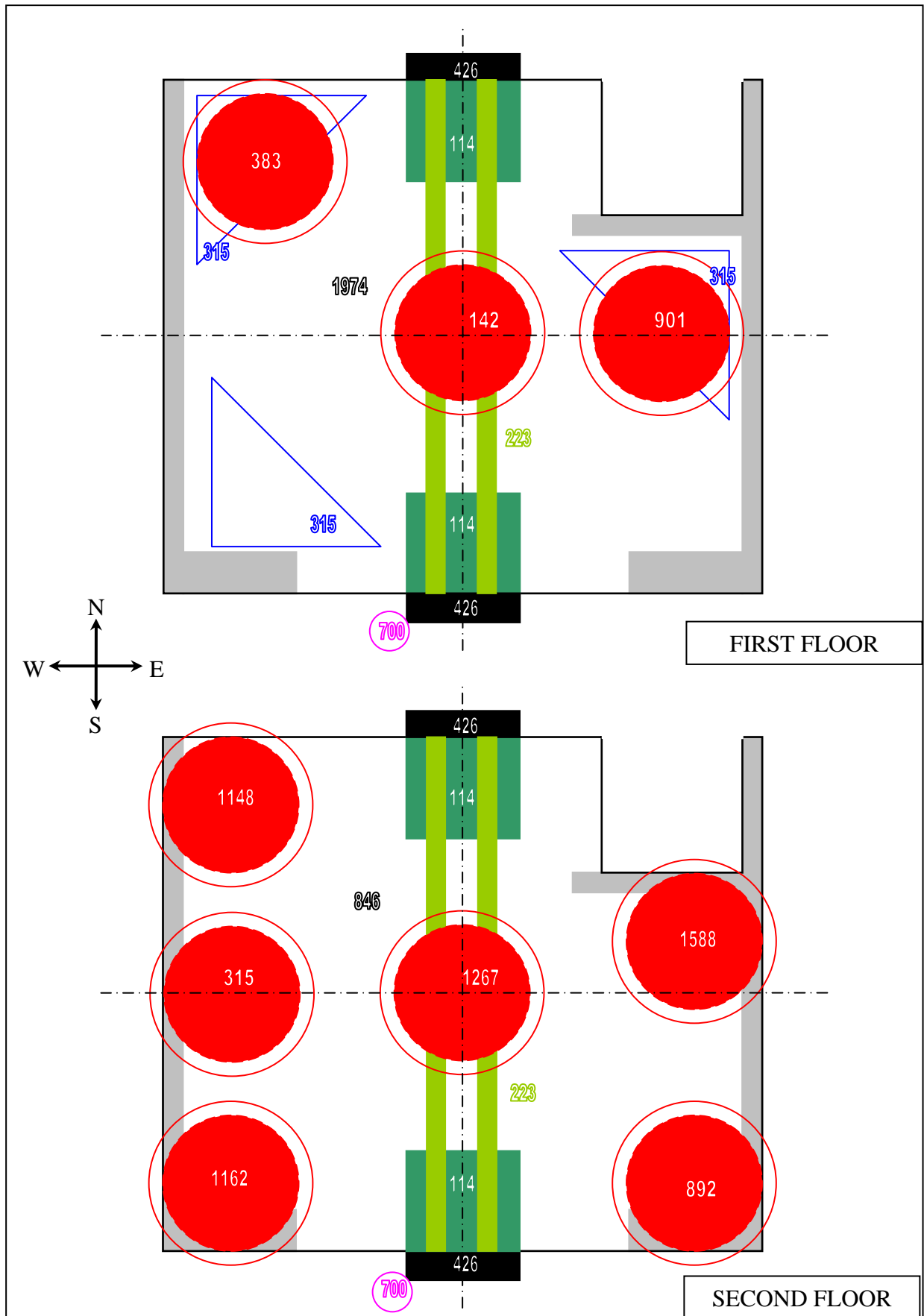


Figure 3– Distribution of the water tanks on the clay specimen

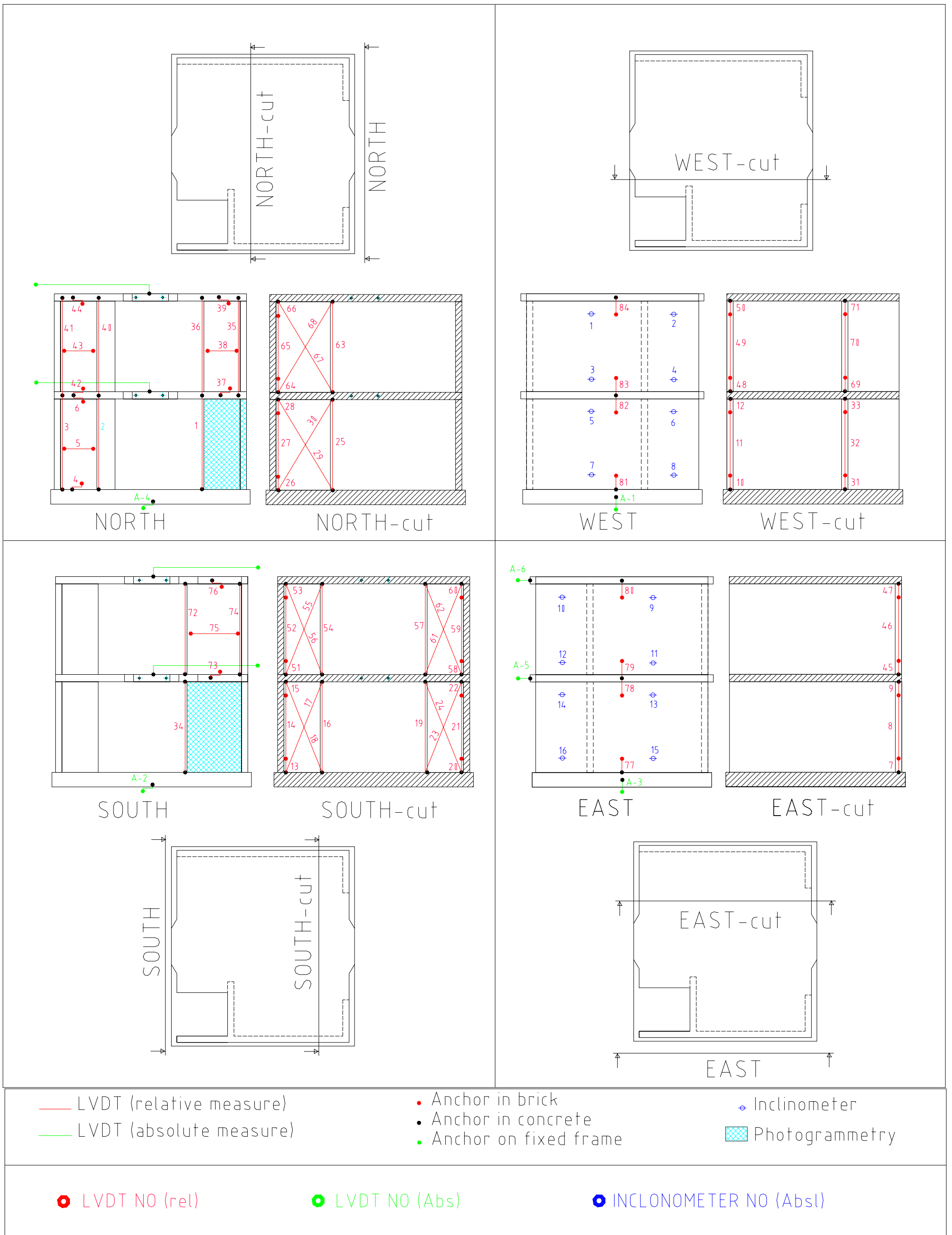


Figure 4: Instrumentation of the calcium silicate specimen

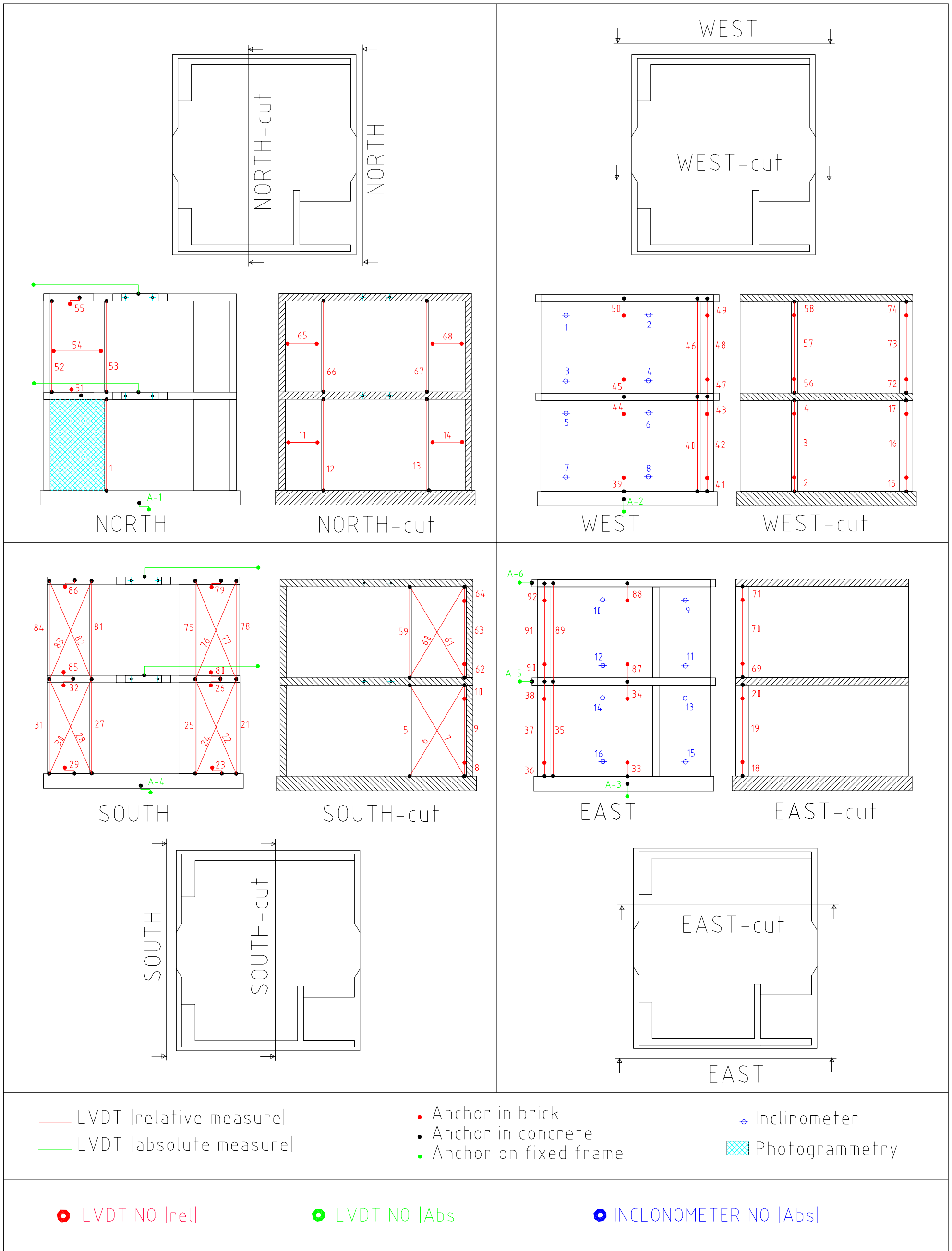


Figure 5: Instrumentation of the clay specimen

3. PARAMETERS USED FOR THE PSEUDO-DYNAMIC TESTS

3.1. Reference accelerogram

The reference accelerogram was a 10 seconds long artificial time history generated to match the EUROCODE 8 design spectrum with the following characteristics:

- Elastic response spectrum of type I
- Peak ground acceleration (PGA) = 0.04g
- Soil type B

The same accelerogram had been used for the series of dynamic tests on the Athens shaking table [2]. The acceleration time history is shown in Figure 6 and the corresponding response spectrum is compared to the target one of EC8 in Figure 7.

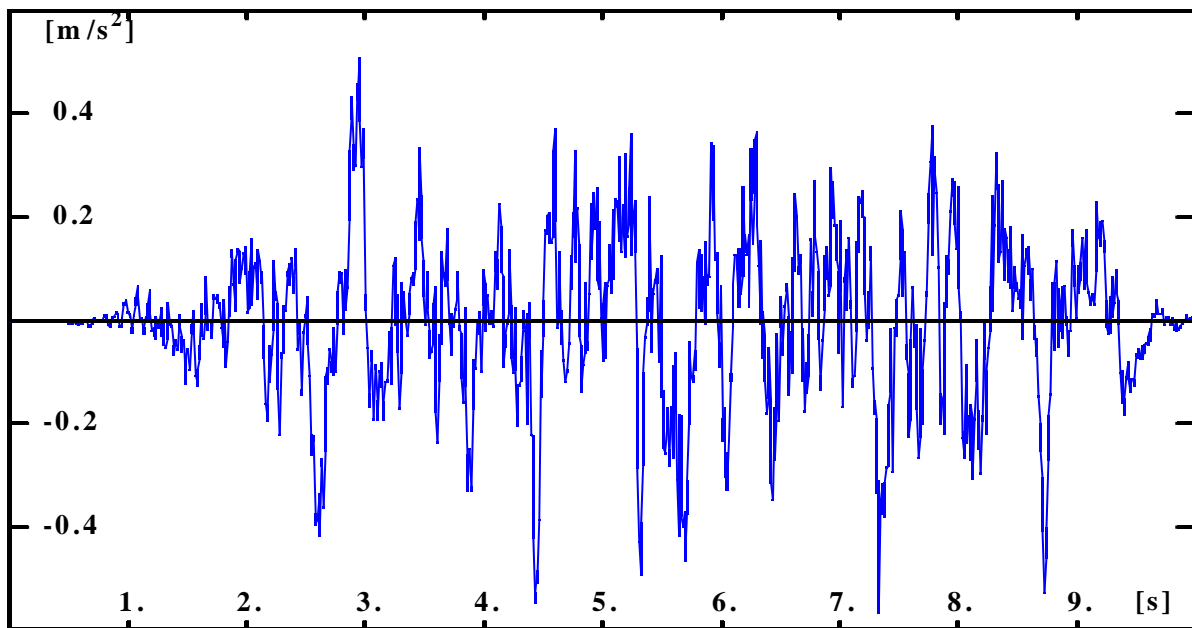


Figure 6: Reference acceleration time history

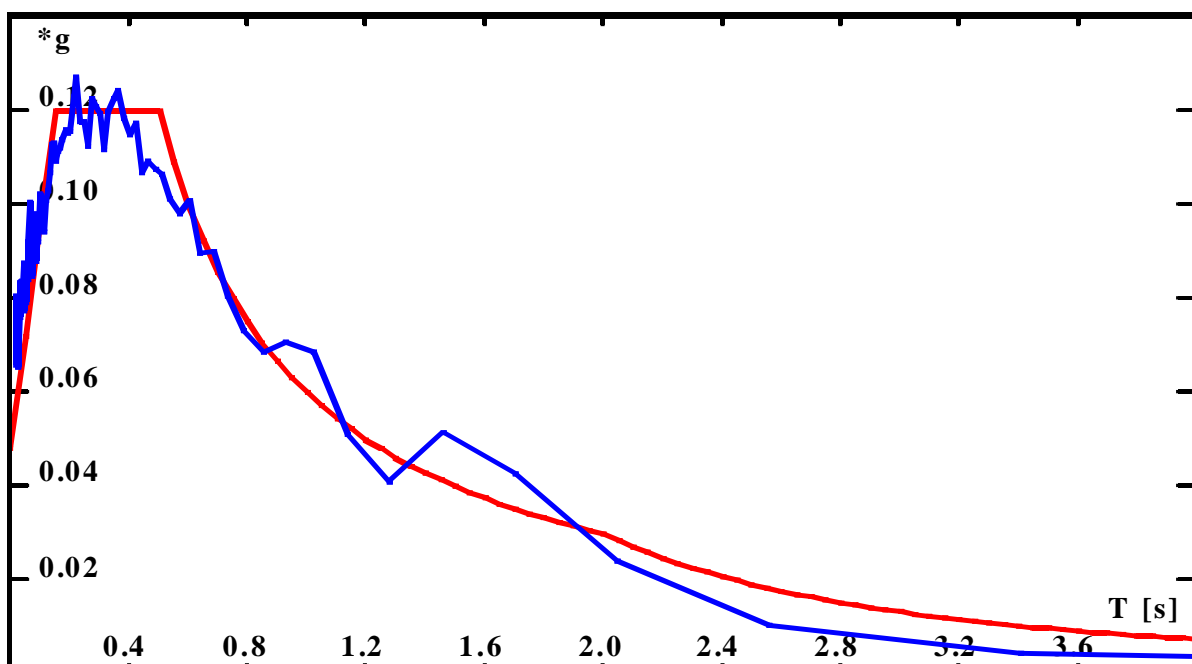


Figure 7: Target (red) and reference (blue) response spectra

3.2. Mass matrix

In a pseudo-dynamic test, the mass matrix may be chosen arbitrarily. In the present case, the specimens to be tested had two degrees of freedom so that a 2x2 mass matrix was required.

The mass matrix has been chosen diagonal: for each degree of freedom (i.e. each floor level horizontal displacement), the mass of half masonry walls below and above the floor (when applicable) has been added to the total mass of each floor slab. Taking 2000kg/m³ as the volumetric mass of the calcium silicate walls, this gives:

- $m_1 = 29000\text{kg}$ for the first floor level
- $m_2 = 26200\text{kg}$ for the second floor level

A slightly different mass matrix has been obtained for the clay specimen because the volumetric mass of the clay masonry walls was then 800, 900 and 1700kg/m³ for the slender, long and shear masonry walls respectively:

- $m_1 = 23900\text{kg}$ for the first floor level
- $m_2 = 23650\text{kg}$ for the second floor level

3.3. Damping

No viscous damping has been introduced in the PsD algorithm. Therefore, the damping measured during the PsD tests was only due to the hysteretic behaviour of the specimens under quasi-static loading conditions. The validity of such a hypothesis may be assessed through comparing the damping values found for the snap-back test on the one hand and for a PsD dynamic test of similar amplitude (~1mm) on the other hand.

3.4. Testing program

Each specimen has been first submitted to a preliminary test (PGA of 0.01g) in order to determine the suitable control parameters (e.g. testing speed) of the continuous pseudo-dynamic method. Then, a series of accelerograms of increasing intensity (0.02g, 0.04g, 0.06g, 0.08g, etc.) have been applied. Each test has been prolonged by 2.5s in order to let the free vibration dampen down after the end of the base acceleration input. The testing program has been stopped just before failure that is when the damage caused to the specimen was so important that a further test could not be safely carried out. The last test performed corresponded to a PGA of 0.20g for the calcium silicate specimen and 0.22g for the clay specimen.

4. PSEUDO-DYNAMIC TEST RESULTS

All the results have been stored in the ELSA database, which is accessible through internet. A login and password can be provided upon request (one for each project partner institution).

The main results of each test are given in annex A (resp. B) for the calcium silicate (resp. clay) specimen. These are the storey absolute displacements and restoring forces time histories and the resulting shear-drift curves of each storey (also disaggregated by side). In all these curves, displacements/drifts and forces/shears are positive when directed towards the reaction wall (west direction in Figure 2 and 3). From these curves, it was possible to identify the time evolution of the two frequencies and of the associated damping ratios: the stiffness and damping matrices of the specimen have been directly identified from the experimental displacements, velocities and restoring forces and then combined with the theoretical mass matrix (spatial model [6]). For the first mode, the evolution of the frequency and damping

ratio is also given in function of the displacement amplitude. Finally, the energy dissipation (by side, by storey and total) is also given as a function of time.

The brief description of the successive tests is given hereafter for each specimen.

4.1. The calcium silicate specimen

During the first two PsD tests (PGA of 0.02g and 0.04g) the structure behaved extremely well in the sense that no damage could be detected (the maximum displacement measured at the top was only 0.8mm and 1.6mm respectively). The first mode was predominant with a frequency around 6Hz and rather low damping (around 2%). However, the responses to 0.02g and 0.04g were not proportional. The non-linearity was probably linked to the “rocking” behaviour of the slender shear walls which can be detected on the shear-drift loops of the ground level, especially on the north side (curved loops with low hysteresis).

During the third test corresponding to 0.06g, the maximum displacement measured at the top has been 2.6mm. For the first time, some noises have been heard (during the two first large cycles). After the test, the specimen has been inspected but only some (flexural) horizontal cracks were visible at the base of the long walls, in both storeys. During the following two tests (0.08g and 0.10g), the maximum displacement measured at the top has been 5.1mm and 7.3mm respectively. Again, some noises have been heard (during the larger cycles) but, after these tests, there were not any significant new cracks.

The first significant damages appeared during the 0.12g test (Figure 8): Large stepwise cracks formed in the west slender wall of the ground floor and, in both long transversal walls, a horizontal crack opened at mid-height of the first level: on the east side in correspondence to the main shear wall, on the west side in correspondence to the slender wall. After an accurate inspection, threadlike stepwise cracks were also detected in the main shear wall of the ground floor. The top displacement reached 16.6mm and the shear-drift curves of the first level were markedly hysteretic owing to the friction along the stepwise cracks.

During the following test (0.14g), the top displacement reached 24.5mm. The existing stepwise cracks were activated (increased residual opening) and new stepwise cracks appeared in the main shear wall and also in the east slender wall of the ground floor. At the upper floor, two horizontal cracks formed in the slender walls, one along the slab-wall joint and the other below the top layer of bricks. New horizontal cracks also appeared in the transversal walls (below the top layer of bricks at each level).

During the test at 0.16g, stepwise cracks appeared in two walls of the first floor (the main shear wall and the west slender wall). The maximum top displacement was 29.3mm

Very few new cracks appeared during the test at 0.18g although the top displacement reached a value of 51.1mm. Conversely, the last test at 0.20g was characterised by a severe cracking (also through the units) of the north-west top corner of the specimen, including the slender wall as well as the neighbouring portion of the transversal wall (Figure 9). The top displacement reached 70.4 mm.

Given the large residual opening of the stepwise cracks in north-west walls, the testing sequence has been stopped also because many of the LVDTs had reached their saturation (some of them had even been damaged).



Figure 8: First relevant damages after the 0.12g test



Figure 9: Damages in the calcium silicate specimen after the final test (0.20g)

The behaviour of the structure under the successive tests may be synthesized in different ways. The top displacement amplitudes are compared in Figure 10, where a clear distinction can be made between the tests up to 0.10g (small amplitudes), the tests 0.12g, 0.14g and 0.16g (medium amplitudes) and the last two tests (large amplitudes).

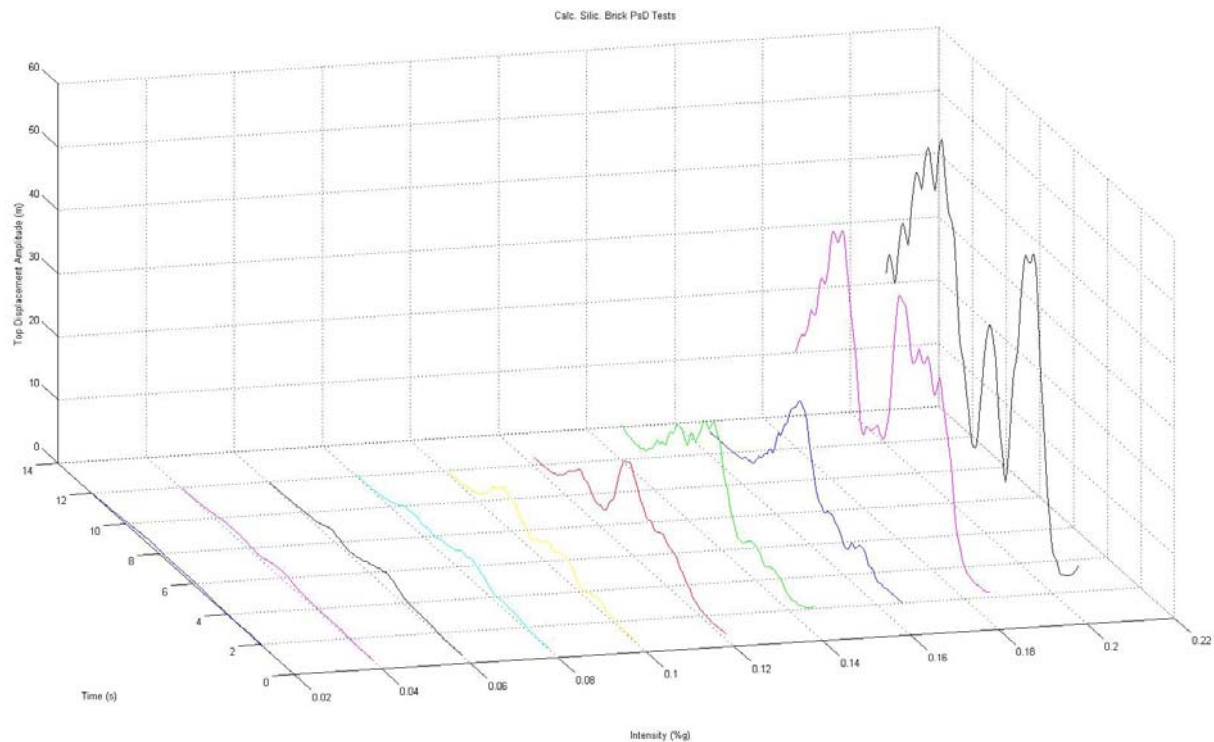


Figure 10 Top displacement amplitudes for the calcium silicate specimen

In Figure 11, the evolutions of the first frequency and of the damping ratio are plotted in function of the displacement amplitude. The first frequency evolution gives a good indication of the progressive stiffness degradation of the structure linked to the crack opening. Until the test at 0.10g, the frequency evolution is almost reversible, while the test at 0.12g (in red) is characterised by a strong frequency decrease which is not recovered at the end. The damping ratio evolution is less clear, especially for large amplitudes. It is stable around 2.5% for amplitudes less than 1mm and increases roughly to 5% for amplitudes up to 5mm.

From the successive shear drift curves, it is possible to derive a rough envelope of the cyclic behaviour of each storey: for each test, the points realising the maximum/minimum shear forces and, if different, the points realizing the maximum/minimum drifts are selected. The results are displayed in Figure 12 and are briefly commented hereafter:

- The drifts reached at the first level are strongly dissymmetric: this is mainly due to a large residual displacement developing from the 0.12g test on.
- The maximum shear force is substantially higher at the lower level and this is clearly attributable to the higher vertical load acting on that level.
- At both levels, the maximum shear force is slightly higher for negative drifts, that is to say when the main shear walls are probably submitted to a higher vertical load due to the overturning moment.
- The first strength degradations appear during the test at 0.12g. However, the drop of strength is rather limited and is partially or totally recovered during the successive tests.
- The curves are characterised by a good ductility characteristic of the stepwise type of failure observed in most of the shear walls.

ESECMaSE ELSA [Calc. Silic. Brick] (63: PsD Model Identified)
 RefD w=100

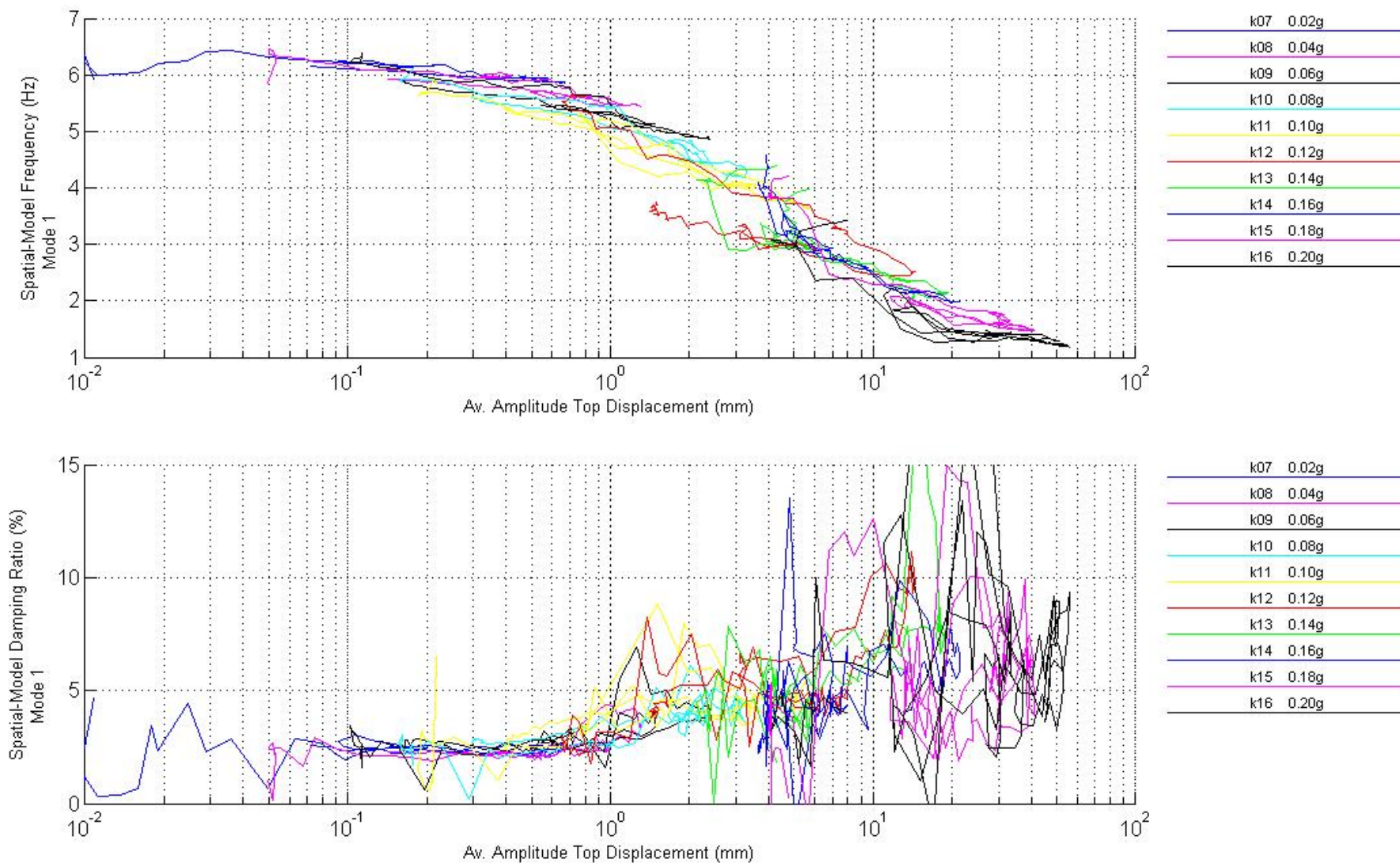


Figure 11: Evolution of the 1st frequency and damping against the top displacement amplitude

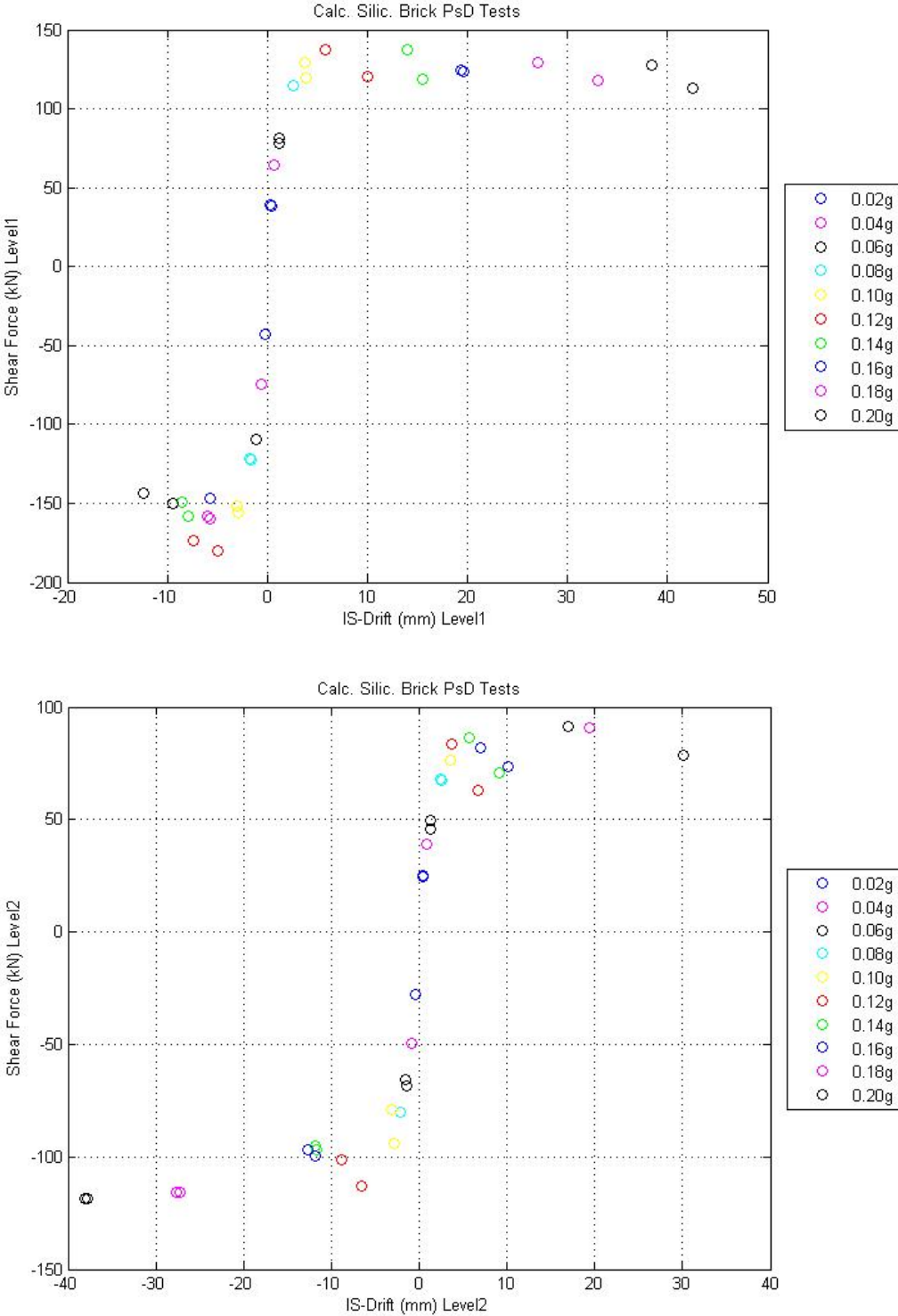


Figure 12: Envelope of the shear drift curves for the calcium silicate specimen

4.2. The clay specimen

It has been rather difficult to detect the cracks in the clay specimen: once closed, the cracks in the bed joint were frequently obscured by the irregular mortar joint.

During the first two PsD tests (PGA of 0.02g and 0.04g), no damage could be detected. The maximum displacement measured at the top was 0.9mm and 1.7mm respectively. The first mode was predominant with a frequency around 5Hz and a damping around 3%. This last value is slightly lower than the 3.5% found during the snap-back test. Again, the responses to 0.02g and 0.04g were not proportional although the shear-drift curves were almost linear.

During the third test corresponding to 0.06g, the maximum displacement measured at the top has been 4.3mm. For the first time, some noises have been heard. After the test, the specimen has been inspected and flexural horizontal cracks were detectable at the base of the long transversal walls, in both storeys.

During the following two tests (0.08g and 0.10g), the maximum displacement measured at the top has been 6.4mm and 10.3mm respectively. Again, some noises have been heard (during the larger cycles) but, after these tests, there were not any significant new cracks.

The first few noticeable damages appeared during the 0.12g test (maximum top displacement of 22.6mm): a horizontal flexural crack opened at mid-height of the first level on the east transversal wall in correspondence to the slender wall. This crack was prolonged by a stepwise crack downwards in correspondence to the main shear wall and was then connected to the existing flexural crack at the base of the wall (Figure 13). Threadlike stepwise cracks were also detected in the east slender wall of the ground floor but their exact extension was difficult to assess (Figure 14, left). Conversely, no damage could be seen in the main shear wall except on the boundaries: cracks had occurred in the bottom joint as well as the lateral vertical joint.



Figure 13: Flexural cracks on the east transversal wall during the 0.12g test

During the following test (0.14g), the top displacement reached 28.0mm. A stepwise crack fully developed in the east slender wall of the ground floor (Figure 14, right). A new horizontal flexural crack opened at mid-height of the second level on the east transversal wall

in correspondence to the main shear wall). This crack was prolonged by a stepwise crack upwards and then by a horizontal crack under the top layer of bricks.



Figure 14: Cracks in the east slender wall of the ground floor after the 0.12g test (left) and the 0.14g test (right)

The test at 0.16g has been very similar to the test at 0.14g in terms of displacement amplitude (28.8mm at the top). However, new flexural cracks opened on the east transversal wall (V-shape stepwise crack in correspondence of the main shear wall visible on Figure 15). Also the junctions between the slender walls and the long transversal walls failed at both levels and several cracks appeared on the lower face of the first slab, mainly parallel to the transversal walls and passing near the corners of the shear walls.



Figure 15: Flexural cracks on the east transversal wall during the 0.16g test

During the test at 0.18g, the top displacement reached a value of 40.9mm. At the ground floor, damages occurred in the main shear wall (diagonal cracks in the top west corner brick prolonged by an uncompleted stepwise crack towards the bottom east corner) as well as in the east slender wall (second diagonal stepwise crack) and in the west one (initial crushing of the top east brick and incomplete stepwise cracks). At the second floor, a stepwise crack formed in the main shear wall (from the top west corner to the east side at 2/3 of the height). Further longitudinal cracks formed on the lower face of the first slab.

During the following test (0.20g), the top displacement reached 62.6mm. All the existing cracks in the long lateral walls were activated with sometimes an impressive opening. A large diagonal stepwise crack and several minor cracks appeared in the east slender wall of the upper floor.

The last test at 0.22g (77.0 mm at the top) was characterised by a severe diagonal cracking (also through the units) of the slender walls of the upper floor (Figure 16 top). Conversely, at the same floor, the main shear wall did not suffer significant additional damage apart from a complete separation along its boundary. At the ground level, the residual opening of the existing cracks had increased and some additional cracks had formed but the load bearing capacity of the three shear walls was still satisfactory. However, given the poor residual bearing capacity of the upper slender walls, the testing sequence has then been stopped.



Figure 16: Damages in the slender walls after the final test (0.22g)



Figure 17: Damages in the main shear walls after the final test (0.22g)



Figure 18: Damages in the slender walls junctions after the final test (0.22g)

The top displacement amplitudes are compared in Figure 19. A clear distinction can again be made between the tests up to 0.10g (small amplitudes), the tests 0.12g, 0.14g and 0.16g (medium amplitudes) and the last three tests (large amplitudes)

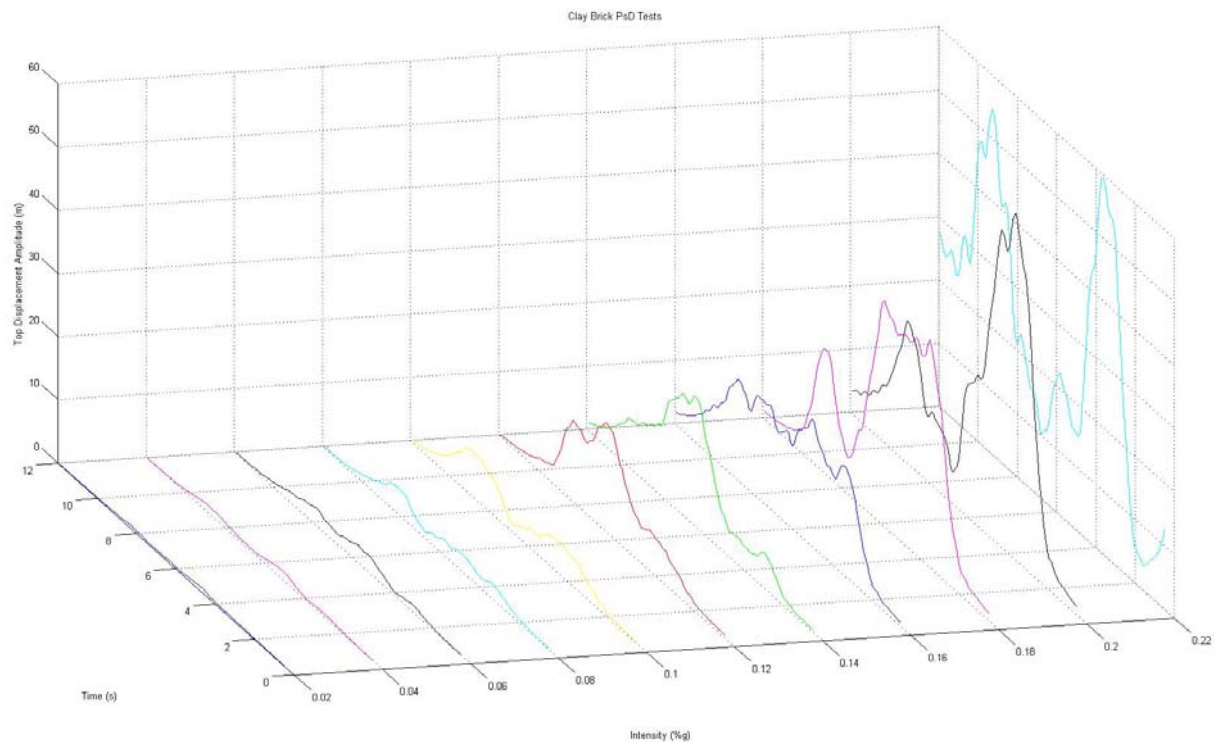


Figure 19- Top displacement amplitudes for the clay specimen

In Figure 20, the evolutions of the first frequency and of the damping ratio are plotted in function of the displacement amplitude. The stiffness degradation is more progressive than in the case of the calcium silicate specimen but the test at 0.12g still appears as the most damaging. Also the damping evolution seems more progressive, starting from 2.5% for amplitudes of 0.1mm, and increasing up to about 4% for amplitudes of 1mm. The interpretation is however raised difficult by the extensive superposition of the successive curves.

The envelope of the cyclic behaviour of each storey is displayed in Figure 21. The curves are very similar to the ones obtained for the calcium silicate specimen, qualitatively and quantitatively:

- The dissymmetry of the drifts reached at the second level is partially due to a residual displacement appearing mainly during the last two tests.
- The maximum shear force is substantially higher at the lower level and this is clearly attributable to the higher vertical load acting on that level.
- At both levels, the maximum shear force is slightly higher for negative drifts, that is to say when the main shear walls are probably submitted to a higher vertical load due to the overturning moment.
- The first strength degradations appear during the test at 0.12g and/or 0.14g. However, the drop of strength is very limited and is totally recovered during the successive tests, except during the last one especially at the second for positive drifts.
- The curves are characterised by a good ductility characteristic of the stepwise type of failure observed in most of the shear walls.

ESECMaSE ELSA [Clay Brick] (63: PsD Model Identified)
RefD w=100

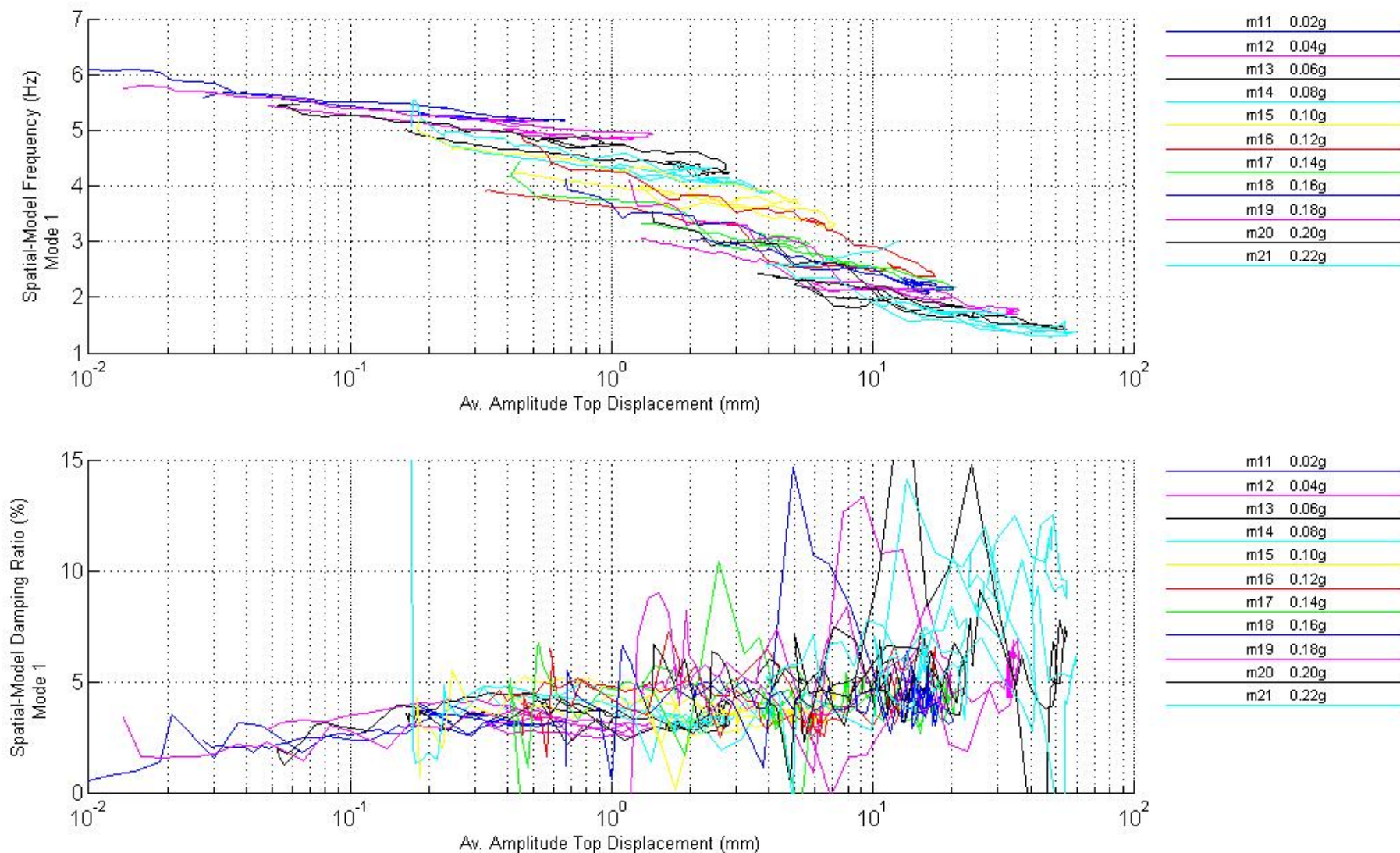


Figure 20: Evolution of the 1st frequency and damping against the top displacement amplitude

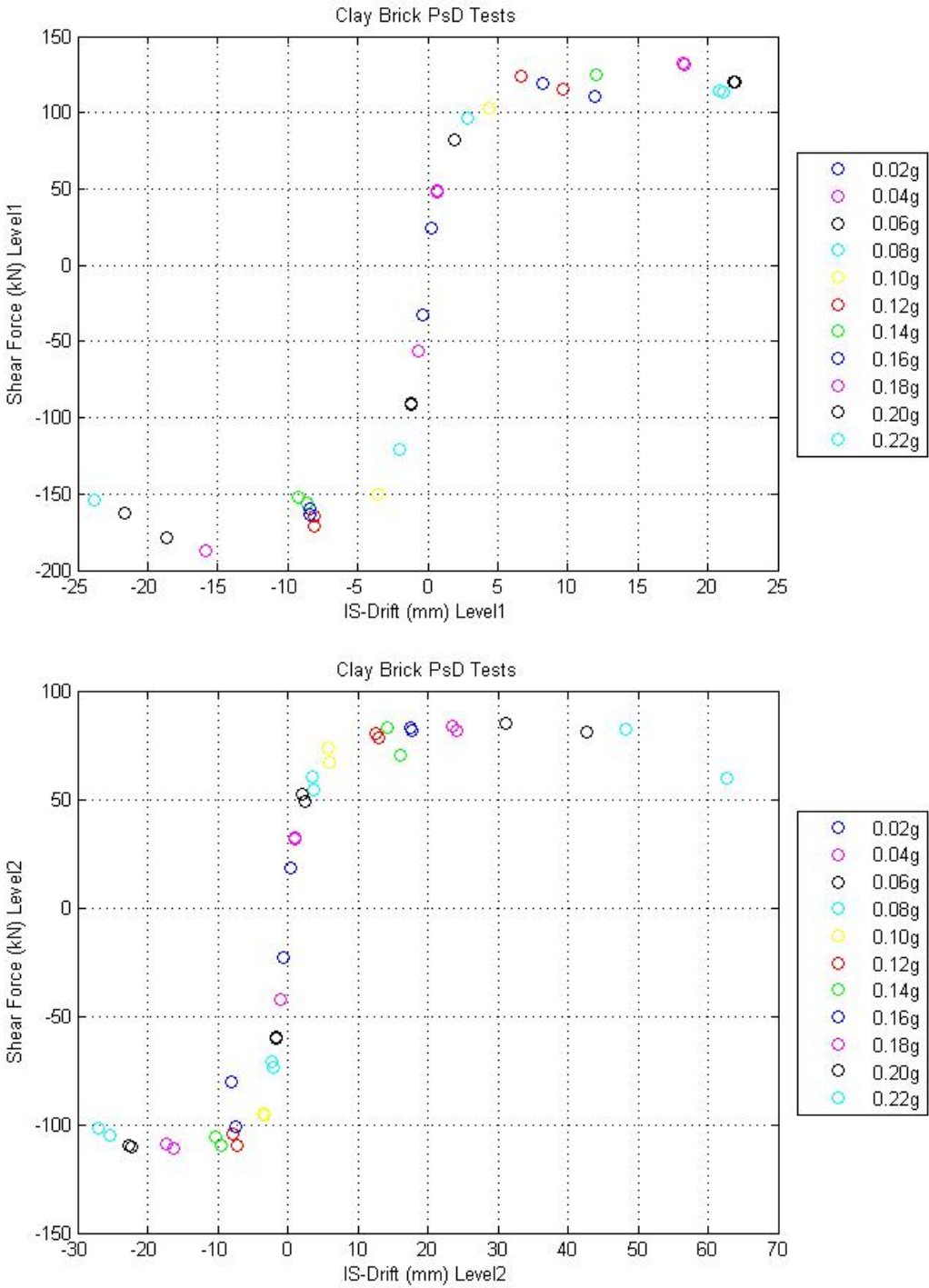


Figure 21: Envelope of the shear drift curves for the brick specimen

5. PHOTOGRAMMETRY

The optical measurement techniques developed at ELSA aim to provide:

- High density optical measurements, in substitution or in complement to the classical local mechanical sensors
- Measurement of displacement/strain fields
- Description of cracking patterns
- Diagnostic on the boundary conditions of an experiment
- Segmentation of the architecture of a mock-up

These techniques need to be adapted to the working conditions of a civil engineering laboratory, characterised by a wide range of sizes and by variations of lighting conditions during an experiment. In addition, they must be sufficiently accurate to detect small deformation on elements undergoing large displacements.

Some first application of photogrammetry at ELSA can be found in [7], where displacement/strain fields and cracks were followed on a flat slab, and in [8] where common low-cost cameras have been used to make stereo photogrammetry.

As mentioned earlier, images of the main shear wall of the ground floor, for both specimens, were taken for all the runs, in synchronization with the classical measurements. In addition, data are available for the north-west slender wall of the ground floor for the calcium silicate specimen, only for 4 first runs. The cameras had Kodak CCD sensors of 1024x1536 pixels, on 4096 levels of gray and were equipped with AF Zoom-Nikkor 24-50mm. In addition a pair of video cameras (Panasonic AW-E350) was used to obtain stereo description of the east transversal walls of both specimens.

Hereafter are presented some results regarding the main shear wall of the ground floor of the calcium silicate specimen. These results are illustrative of the potentialities of the method.

5.1. Segmentation into bricks, texture and targets segregation

The wall to be monitored was prepared as follows:

- A random, sufficiently dense pattern has been deposited on the whole face so that any point of its surface could be investigated afterwards. Black and white paints were used to enhance the spectrum of luminance and to obtain high contrast in the patterns.
- Targets of various sizes have been positioned along the brick joints (15.2mm targets) and the wall perimeter (29.3mm targets) so that structural discontinuities could be easily processed from these initial master measurements.

A close-up view of the wall is given in Figure 22 (top east corner), where the initial grey background can be seen with black and white projected paint. The two types of targets are also visible. In particular, one big target is attached to the east transversal wall (one can notice its shadow projecting on the main shear wall) while another big target is stuck directly on the brick.

Sequences of 200 images were taken before and after each run, in order to obtain reference images – thus at a reduced noise - by averaging them. The reference image corresponding to the initial state before the run was used to sample the various patterns to be tracked in the successive frames of the test. It was also used as the basis of brick segmentation. This was obtained through a succession of mathematical morphology operations [9], which will not be described here.

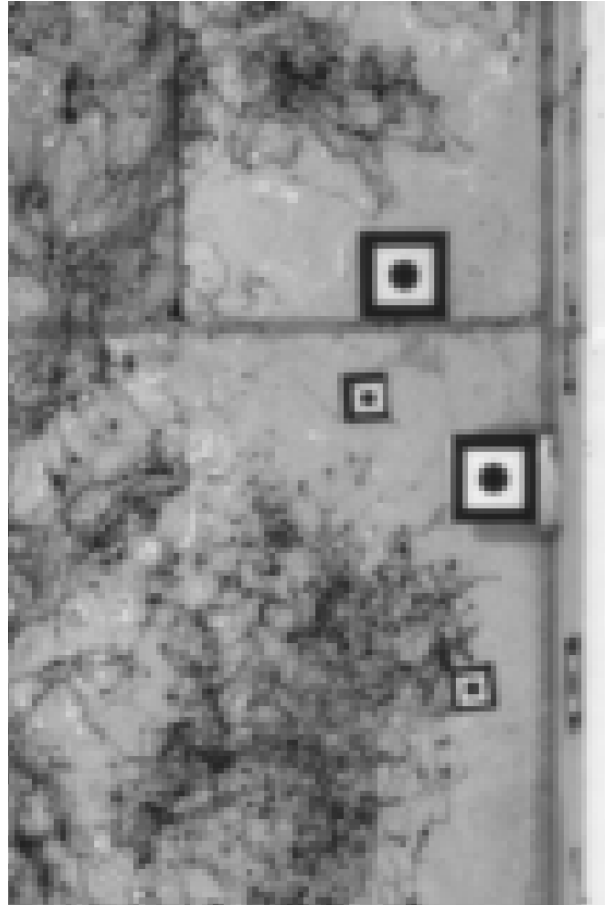


Figure 22- Close-up view of the artificial texture and targets deposited on the wall

The targets were segregated semi automatically in the following way: a representative target was cropped from the reference image, and this characteristic pattern was correlated with the whole image. The regional maxima of the correlation function were sampled and sorted by decreasing value. The majority of the targets could be segregated by threshold of the correlation product, the rest of those being selected by hand, with help of an ad-hoc graphical user interface.

The whole field of view is presented in Figure 23, in which the segmentation into bricks appears in red while the targets used for optical measurements are coloured in green. Special targets, identified by a different colour, will be used as reference (horizontality) or for comparison with transducer measurements (LVDT or HEIDENHAIN).

Six small targets have been stuck on each bricks. The network of targets is irregular, but its topology allows the monitoring of the opening/closure of the horizontal/vertical joints, the targets being stuck in vis-à-vis on each neighbouring pair of bricks. It also allows the detection of strains in the brick by computing the relative displacements of the three pairs of targets stuck on each brick. Possible missing targets in the network can be easily replaced by the artificial texture deposited on the target location. The bottom right part of the wall is blinded by the anchoring of the slab onto the strong floor, but this does not impair too much the measurement as this 'black zone' is quite small and located in a region of small displacements.

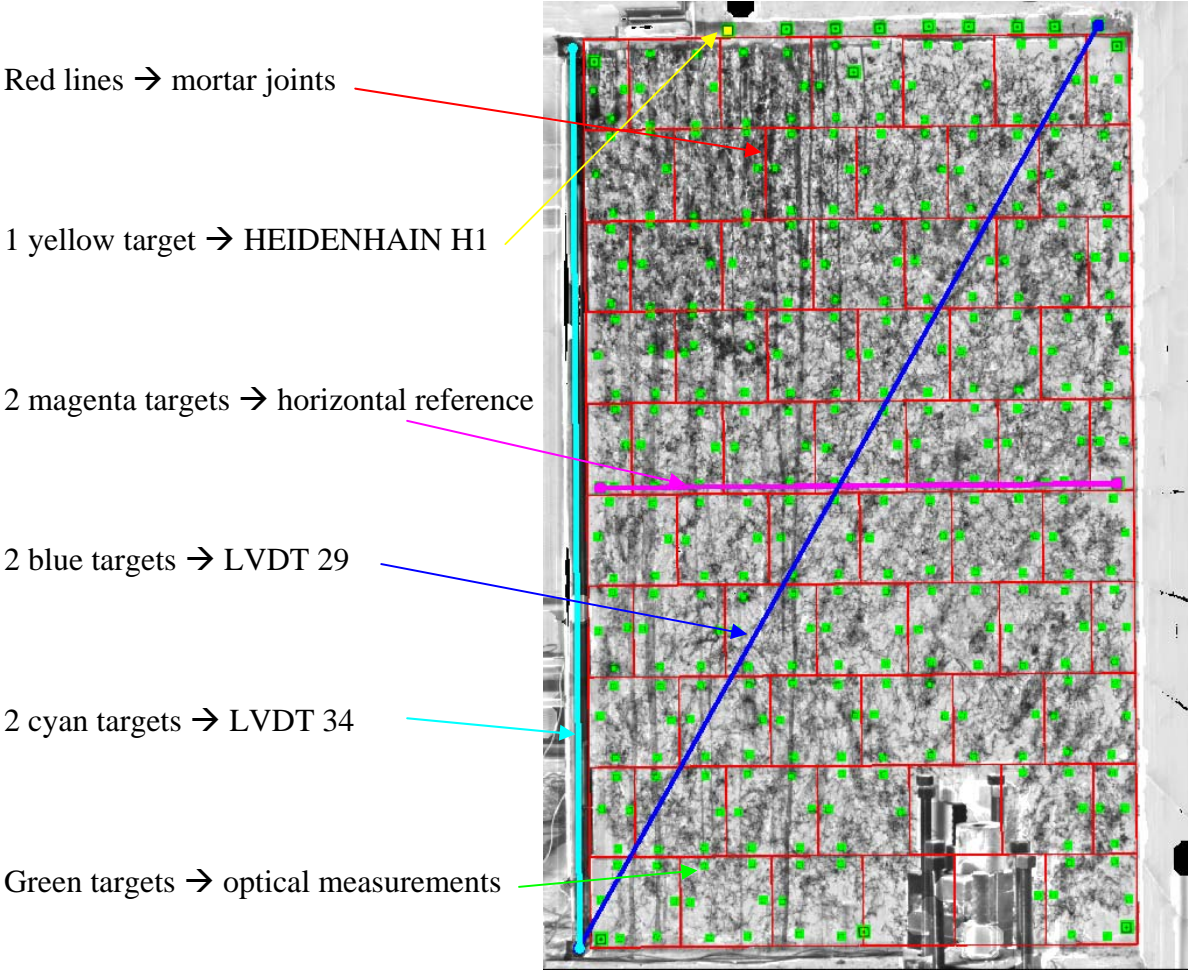


Figure 23- The main shear wall after segmentation and segregation

5.2. Calibration and tracking process

The calibration of the camera and optics is made directly on the experimental set-up. The matlab software provided by Bouguet [10] has been used to evaluate the parameters characterizing the camera and its optics, and the position of the camera with respect to the wall. The method is based on a set of 50 to 100 images of a chessboard -of perfectly known geometry- positioned at various orientation and distance from the camera. By comparing each of these images with a reference shot of the scene without chessboard, a network of points having their physical coordinates in the chessboard frame coinciding with their pixel coordinates in the image frame can be identified. From this set of validated network points, Bouguet’s code delivers the focal length and the distortion parameters of the optical system. The distortion has been found negligible in first approximation so that no correction was needed. In addition, the relative position of the wall plane with respect to the camera was obtained by considering the images in which the chessboard was laying on the wall face. Finally, two targets (magenta colour in Figure 23) have been chosen as indicative of horizontality so as to complete the reference frame of the wall.

The measurements that will be presented in the following result exclusively from the processing of the target network. The total number of targets tracked during each experiment may slightly vary from run to run, because the network has been enriched or completed from test to test. But the mean number of targets to be considered is 360 elements per run.

The tracking method used in this study is described in [11]. Sub-windows of interest -e.g. targets- are sampled in the reference image: these templates must be tracked over time, on the successive frames of the run. In the case of concern, the patterns to be followed rotate and translate as function of time, with varying light conditions but very slight deformations. These transformations of the initial, reference template are modelled by 8 parameters: 2 parameters for the translation, 4 parameters for linear transformation and 2 parameters for the lighting conditions. The cost function, which is the squared difference between the template and the current image, is minimized with respect to these 8 parameters. As the reference template is interpolated by C3 thin plate spline functions, the cost function is an analytical of the transformation parameters and a classical Newton-Raphson technique could be used for minimisation at each step. The gradient and the Hessian matrix involved in this optimisation process are straightforwardly derived, at any parameter point, from the interpolated cost function, and sub pixel approximation is naturally introduced in this way.

5.3. Comparison with transducer measurements

The records of three transducers (HEIDENHAIN H1 and LVDTs 34 and 29) are hereafter compared with the optical measurements. The selected targets, shown on Figure 23 (in yellow, cyan and blue respectively), did not coincide with the extremities of the transducers but were the best available. More precisely, the HEIDENHAIN H1 was attached on the south border of the slab (not visible in Figure 23) while the yellow target was fixed onto the slab near the shear wall; the LVDT 34 was parallel to the west side of the wall (visible in Figure 23) and the cyan targets were placed near its extremities, fixed on the concrete slabs; the LVDT 29 was on the north (hidden) face of the wall while the blue targets were on the south face and fixed to the concrete slabs.

The H1 signal is compared to the optical signal for the test at 0.02g for which the maximum horizontal displacement at the first level was less than 0.4mm, i.e. a fourth of a pixel in the images. The optical signal was very noisy and had to be filtered by Haar wavelets. The filtered signal compares well with the H1 signal (Figure 24). The difference signal has a flat spectrum, typical of white noise. This difference might be due to the optical procedure itself or to the fact that the HEIDENHAIN signal results from an average over each time step whereas the optical signal is an instantaneous measure at the beginning of each time step.

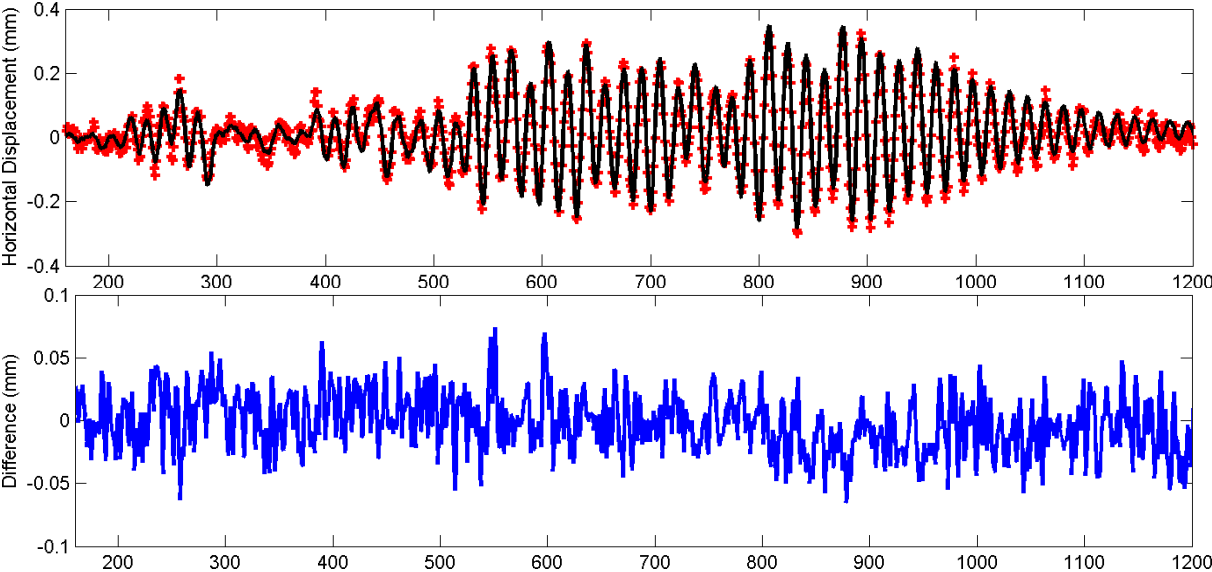


Figure 24 – H1 (black), optical signal (red crosses) and difference (blue) for 0.02g

Better results were obtained for large amplitude tests (Figure 25). The HEIDENHAIN and optical signals are well correlated and the difference signal is of the same form/magnitude as before (white noise of less than 0.1mm) except during the first large cycles. The greater differences then observed might be due to the deformation of the slab.

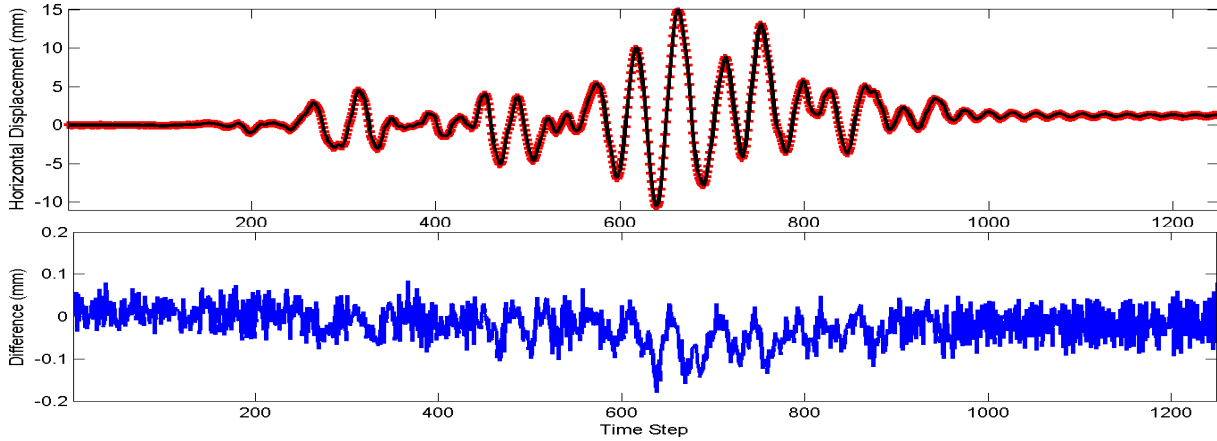


Figure 25 – H1 (black), optical signal (red crosses) and difference (blue) for 0.16g

The LVDT 34 signal is compared to the optical signal for the test at 0.12g (0). The agreement is excellent in the positive range (elongation of the LVDT) whereas in the negative range, the signals exhibit discrepancies, the LVDT signal being systematically higher, in absolute value, than the optical signal.

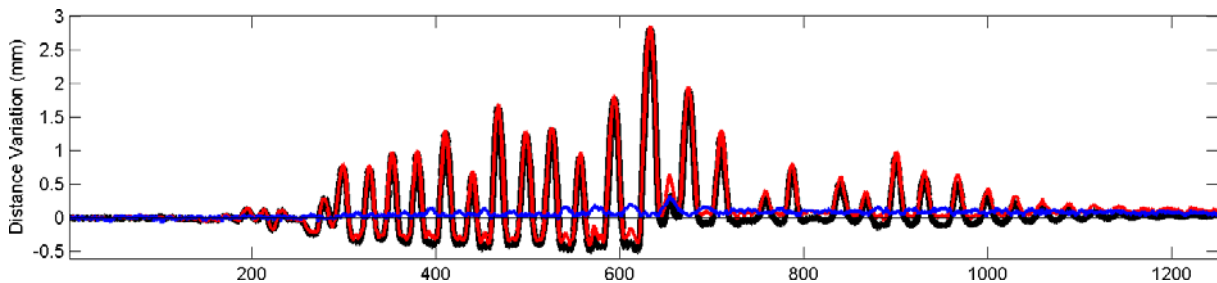


Figure 26– LVDT 34 (black), optical signal (red) and difference (blue) for 0.12g

The same remark holds true for Figure 27 where the LVDT 29 signal is compared to the optical signal for the test at 0.16g. This difference might be linked to a malfunction of the LVDT but need to be further investigated.

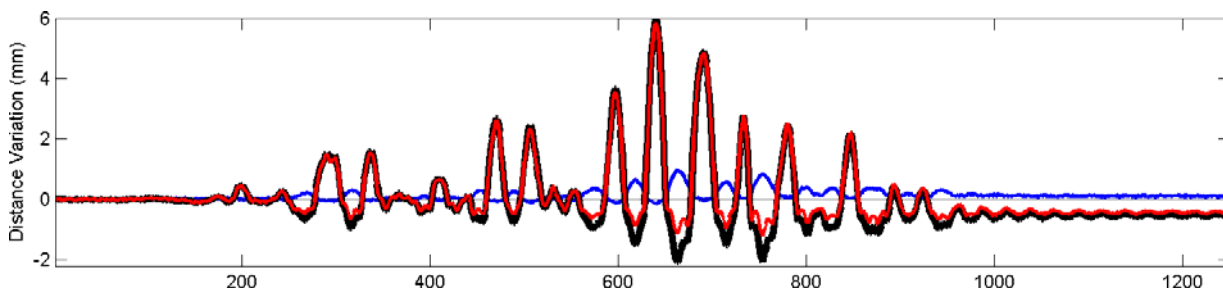


Figure 27 – LVDT 29 (black), optical signal (red) and difference (blue) for 0.16g

5.4. Displacement fields

The displacement signals measured on each target provide a network of points at each time step. This network has been interpolated with Delaunay triangulation, for a certain number of time steps in various runs. In Figure 28 to 31, successive horizontal and vertical displacement fields are visualized at different time steps during the test at 0.12g. The colour encoding is proportional to the displacement amplitude: red for positive maxima, green for zero values, blue for negative minima. Displacements are positive when directed to the right or upwards. Four profiles of displacements are also superimposed so as to facilitate the interpretation of the maps. The time history of horizontal and vertical top displacement (yellow target in Figure 23) is given respectively on the left side and on the bottom side. On these curves, the selected time step appears as the limit between the red and blue colours.

The obtained displacement fields are very helpful for identifying the behaviour of the wall. In particular, it is possible to identify precisely the location and amplitude of the cracks, well before they become visible to the naked eye.

In Figure 28, the horizontal displacement is 5mm towards left. At this stage of the test, the maps indicate a pure rocking behaviour of the wall around its bottom left corner. Soon after, for the next displacement peak in the opposite direction, the displacement field is completely different (Figure 29): the rocking behaviour around the bottom right corner is combined with a multiple stepwise cracking along the compressed diagonal.

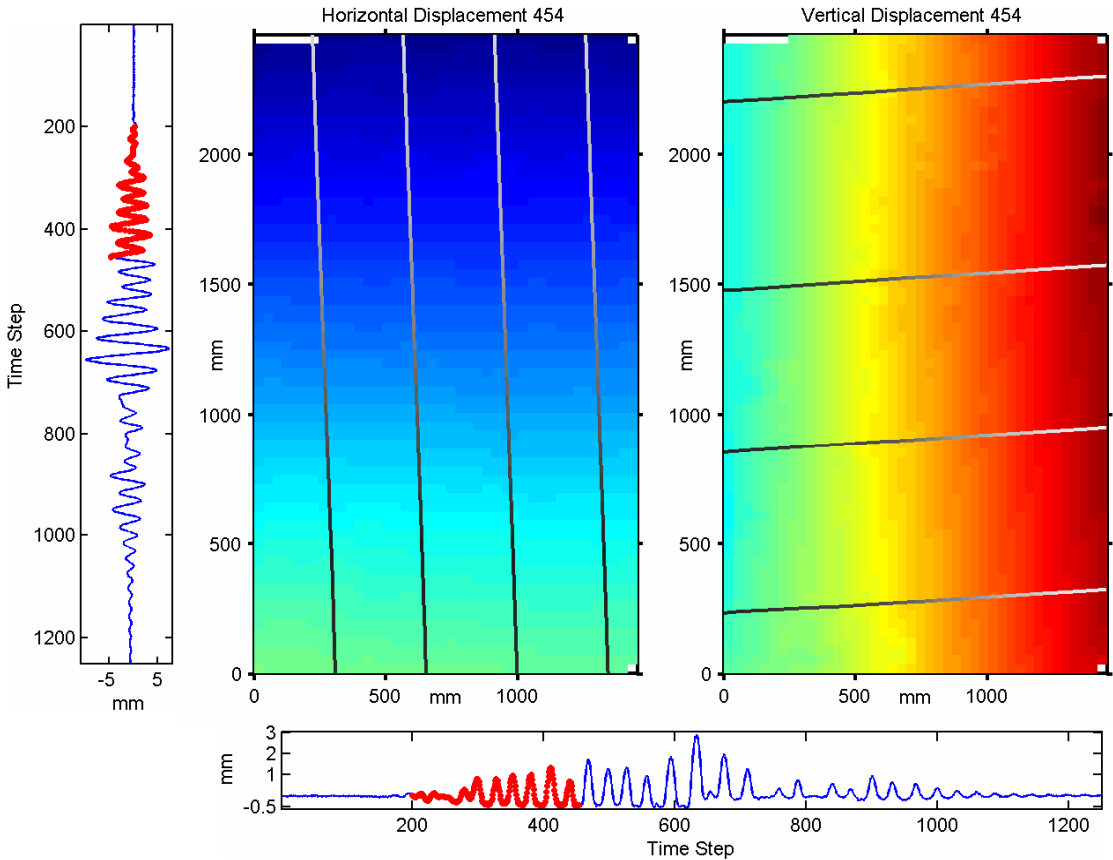


Figure 28 - Pure rocking behaviour of the wall

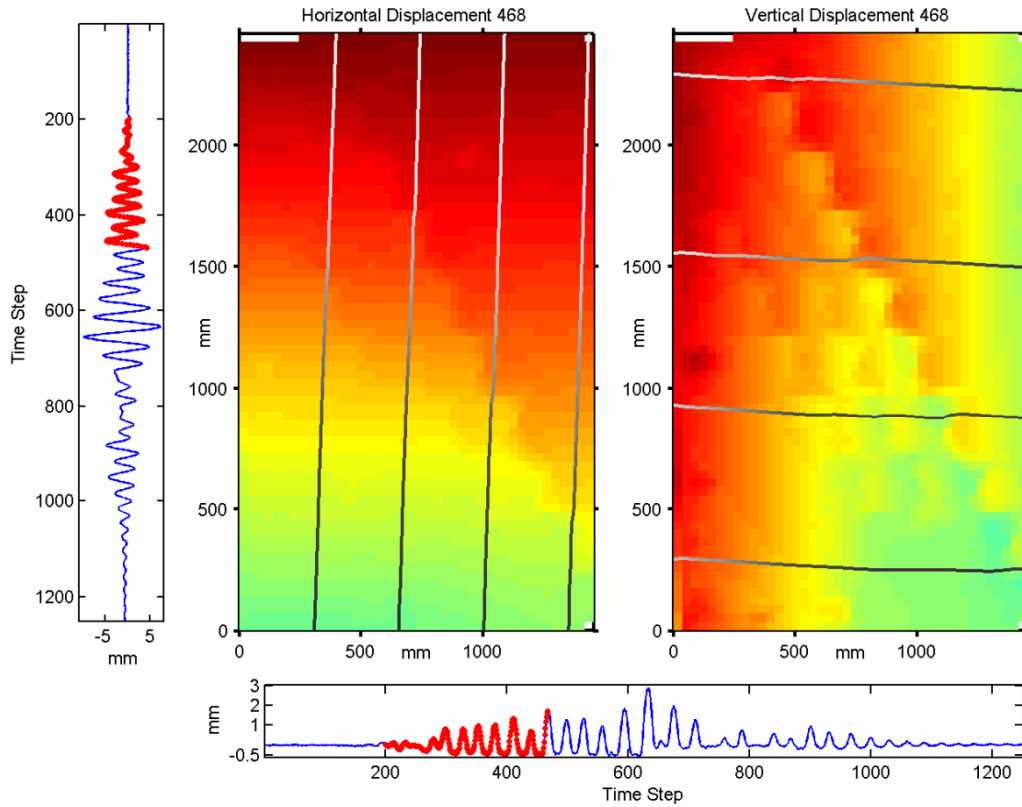


Figure 29 - Primary stepwise crack initiation along the compressed diagonal

At a later stage, a stepwise crack fully develops in the opposite direction, from the bottom left corner to the right mid-height, that is to say in correspondence of a bed joint flexural crack in the long transversal wall (Figure 30).

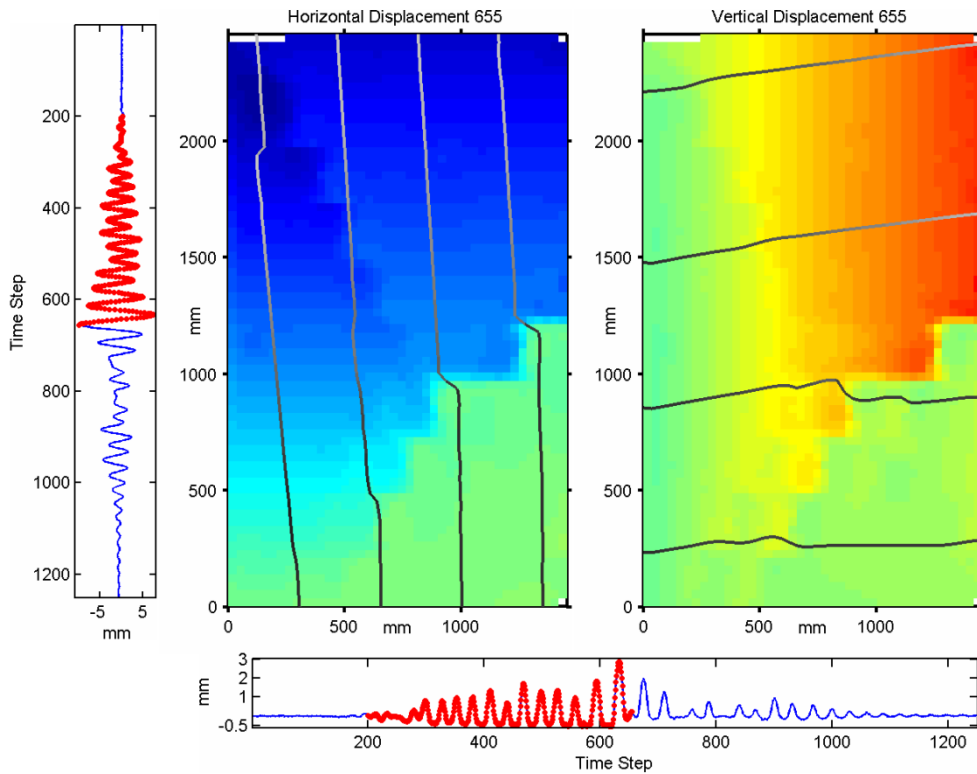


Figure 30 - Secondary stepwise crack at mid-height

The displacement maps then indicate a quasi rigid rotation of the upper part of the wall around the bottom left corner, the lower part being motionless. The first diagonal crack is then hardly visible, proving the nearly complete closure of the corresponding cracks. For the next displacement peak in the opposite direction, the situation is similar with respect to the first diagonal crack: the upper part of the wall is rotating around the bottom right corner whereas the lower part is almost motionless. Again the other diagonal crack is hardly visible.

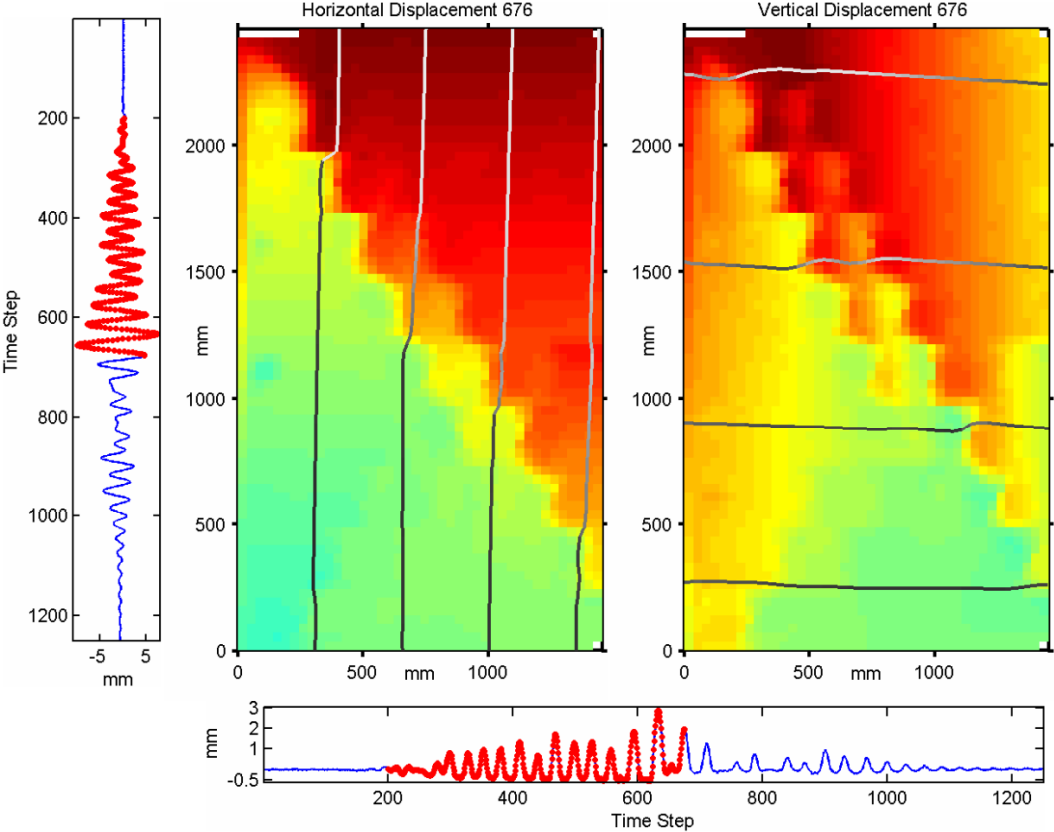


Figure 31 Primary diagonal stepwise crack fully developed

The last map of horizontal displacement, shown in Figure 32, exhibits a characteristic “egg timer” shape. Basically, the wall is separated into four parts by an X stepwise crack. The top (resp. bottom) part does not exhibit residual displacement as it is linked to the top (resp. bottom) slab. The left (resp. right) part exhibits a negative (resp. positive) residual displacement associated to a rigid rotation around the bottom left (rep. right) corner, implying thus a residual opening of the cracks. The dissymmetry of the cracking pattern is due to the interaction with the transversal wall present on the right side.

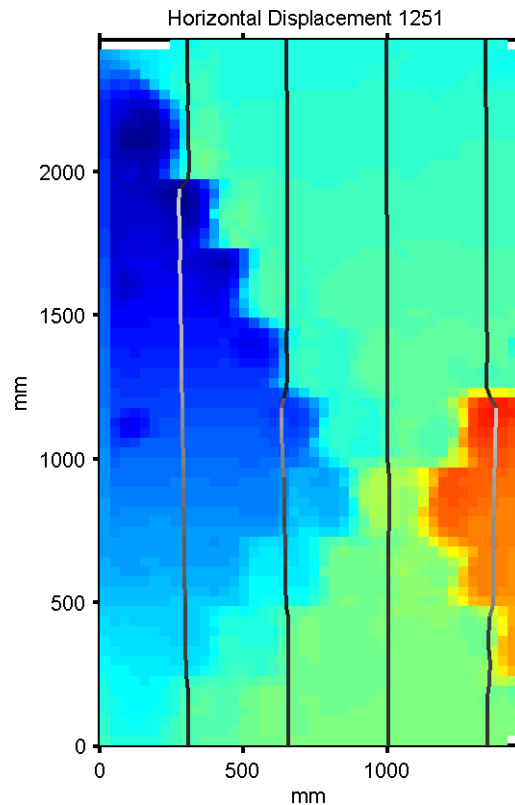


Figure 32 - Residual horizontal displacement field after test at 0.12g

6. CONCLUSION

Both specimens sustained the 0.10g test without suffering relevant damages (only flexural cracks at the base of the long transversal walls). In both cases, the first significant damages have been observed during the 0.12g test and have been accentuated by the 0.14g test. However, the failure modes observed (stepwise cracks in the in-plane walls and horizontal cracks in the bed joints of the transversal walls) were associated to a ductile behaviour so that the specimens could sustain further testing until 0.20g for the calcium silicate specimen and 0.22g for the clay specimen. It should be however mentioned that the PsD method prevents local vibrations/failures (observed in the shaking table tests) and the (out-of-plane) failure linked to the local inertial forces of the bricks. The PsD results may therefore overestimate the earthquake resistance of the specimens especially once extensive cracking has occurred in the longitudinal and transversal walls.

7. REFERENCES

- [1] Joint Research Centre, “Definition and design of the test specimen”, Deliverable D8.1, 2007.
- [2] National Technical University of Athens, “Test results on the earthquake resistance on improved masonry materials by shaking table tests”, Deliverable D7.2a, 2007.
- [3] University of Pavia, “Test results on the behaviour of masonry under static cyclic in plane lateral loads”, Deliverable D7.1c, 2008.
- [4] Commission of the European Communities, European Committee for Standardization, “EN 1998. Eurocode 8: Design of structures for earthquake resistance”.

- [5] Anthoine, A. and Molina, F.J., “Pseudo-dynamic testing of full scale masonry structures: preparatory work”, 12th International Brick/Block Masonry Conference, Sydney 18-20 February 2008.
- [6] Molina, F. J., Pegon, P. and Verzeletti, G., “Time-domain identification from seismic pseudodynamic test results on civil engineering systems”, 2nd International Conference on Identification in Engineering Systems, University of Wales Swansea, March 29-31 1999.
- [7] Capéran, Ph. (2007). “Displacement and Strain Field Photogrammetric Measurements of a Reinforced Concrete Slab Submitted to an Earthquakes Loading,” Proceedings of the OPTIMESS2007 Workshop, Leuven, Belgium, May 28-30, 2007.
- [8] Lathuilière, A.-C. and Capéran, P., (2007). “Use of Low-cost Digital Consumer Camera for Stereo-photogrammetry of Structures Undergoing Destructive Tests,” Proceedings of the OPTIMESS2007 Workshop, Leuven, Belgium, May 28-30, 2007.
- [9] Soille P. Morphological Image Analysis. Springer, 2003.
- [10] Bouguet, J. Y. (2007). “Camera Calibration Toolbox for Matlab,” Web page: http://www.vision.caltech.edu/bouguetj/calib_doc/index.html
- [11] Capéran, Ph. (2007c). “A New Tracking Algorithm with Application to a Practical Measurement Case,” Proceedings of the 8th Conference on Optical 3-D Measurement Techniques, Zurich, Switzerland, July 9-12, 2007.